Check for updates

Preparation and anti-oxidation performance of Al$_2$O$_3$-containing TaSi$_2$–MoSi$_2$–borosilicate glass coating on porous SiCO ceramic composites for thermal protection

Xiafei Li, Junzong Feng,* Yonggang Jiang, Hao Lin and Jian Feng [ID] *

In order to improve the thermal oxidation resistance of carbon fiber-reinforced porous silicon oxycarbide (SiCO) ceramic composites, an Al$_2$O$_3$-containing TaSi$_2$–MoSi$_2$–borosilicate glass coating was formed on the surface of the composites *via* brushing and sintering. The anti-oxidation property of the coated composites at 1873 K was investigated. Microstructures and chemical compositions of the sample before and after anti-oxidation test were determined using XRD, SEM and EDS. After heating in air at 1873 K for 20 min, the Al$_2$O$_3$-containing TaSi$_2$–MoSi$_2$–borosilicate glass coating effectively protects the SiCO ceramic composites and the coated sample kept its appearance well without obvious defects on the surface. The cross-sectional SEM images show that the coating is covered by a film of oxidation products with a thickness of about 40 μm, which is dense and crack free. Inside the A-TMG coating, irregular-shaped silicides are surrounded by continuous borosilicate glass and no penetrating holes or visible cracks are found. Al$_2$O$_3$ increases the viscosity of the borosilicate glass, which improves oxidation resistance of the coated sample by enhancing gas-penetration resistance of the glass. In contrast, the sample without Al$_2$O$_3$ in the coating slurry is severely oxidized and exhibits lots of open pores on the surface after oxidation test.

1   Introduction

With hypersonic aircrafts reaching the speed of Mach number 10 and above, the temperature of windward surface can rise up to 1873 K correspondingly.[1–3] Therefore, this poses a severe challenge to the thermal protection system of the aircrafts, for which thermal protection materials with high temperature resistance, low thermal conductivity, excellent anti-oxidation and anti-ablation performances are urgently required.[4,5] Silicon oxycarbide (SiCO) ceramic composites reinforced by hard carbon felts are considered as one of the most promising candidates. It has advantages of rigid thermal insulation, light weight, low thermal conductivity, as well as the ability to retain its strength and shape when exposed to oxidizing environment at above 1873 K because of the extremely high temperature resistance of the hard carbon felts.[6–8] However, the porous structure of SiCO ceramic composites causes oxygen to diffuse easily, which significantly weakens the oxidation resistance of the composites and limits its application in oxidizing environment at high temperature.[9,10] Therefore, anti-oxidation coating

is urgently needed for porous SiCO ceramic composites to prevent degradation.[11,12]

With continuous improvement of the performance of the rigid thermal insulation, the matching surface-thermal-protection coating is also developing. The single-phase glass coating, reaction cured glass coating (RCG), toughened uni-piece fibrous insulation coating (TUFI) and high-efficiency tantalum-based ceramic composite (HETC) have been investigated successively.[13] According to the US patents,[14,15] the multilayer structure of single-phase glass coating needs to be sintered repeatedly and has a poor thermal shock resistance. RCG is applied on the first generation of rigid thermal insulation (LI). However, the mismatch of the thermal expansion coefficients between the RCG and the substrate has not been completely solved.[16–20] TUFI is mainly applied in the second generation of rigid thermal insulation (FRCI and AETB), and the gradient coating has high impact toughness and good thermal shock resistance. However, both RCG and TUFI are SiO$_2$-based coatings, so the utility temperature is limited by the glass yield point.[19,21,22] HETC is the latest generation of coating technology, which was applied in the toughened uni-piece fibrous reinforced oxidation-resistant composite (TUFROC) developed by NASA Ames Research Center.[23–26] Main components of HETC include TaSi$_2$, MoSi$_2$ and borosilicate glass (B$_2$O$_3$ and SiO$_2$), as well as a small amount of SiB$_6$ as the processing aid. Both TaSi$_2$

Science and Technology on Advanced Ceramic Fibers and Composites Laboratory, National University of Defense Technology, 109 De Ya Rd, Changsha, Hunan, 410073, P. R. China. E-mail: fengj@nudt.edu.cn; junzongfeng@nudt.edu.cn
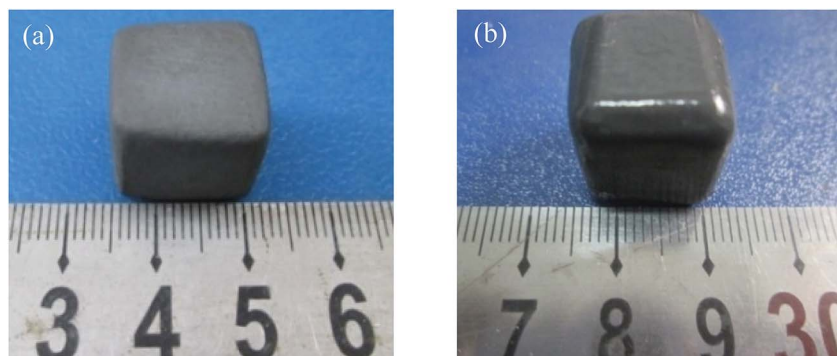
Fig. 1 Photographs of TMG coated sample (a) and A-TMG coated sample (b).

and $MoSi_2$ possess high melting points ($TaSi_2$: 2473 K, $MoSi_2$: 2293 K) and low density ($TaSi_2$: 9.14 g cm^{-3}, $MoSi_2$: 6.24 g cm^{-3}). In this coating, they are used as emittance agent. Besides, $MoSi_2$ is also used as an absorbent of oxygen to reduce oxidation rate of $TaSi_2$.[27] HETC has a high-emittance and low-catalytic-efficiency surface. Moreover, it shows excellent thermal shock resistance and ablation-resistant characteristics in a heat flux in excess of 300 W cm^{-2}.[28–30]

Due to successful application of HETC, many researchers have studied the high-emissivity coating.[31–35] Tao *et al.* prepared the $TaSi_2$–$MoSi_2$–borosilicate glass coating on mullite fibrous ceramics to enhance surficial thermal radiation and investigated the effects of $TaSi_2$ dosages on the coating structure,

phase composition and thermal shock resistance.[36] Shao *et al.* reported a $TaSi_2$–$MoSi_2$–borosilicate glass coating on fibrous ZrO_2 ceramic, whose emissivity is up to 0.9 in the range of 0.3–2.5 μm and exhibited excellent thermal shock resistance.[37] Wang *et al.* introduced 1 wt% Al_2O_3 whiskers to $MoSi_2$ coating, and significantly improved its oxidation resistance. The mass loss of the coated material was only 0.17% after heating at 1723 K.[38] In this paper, Al_2O_3 was added into the SiO_2–B_2O_3 borosilicate glass to increase its viscosity and the $TaSi_2$–$MoSi_2$–borosilicate glass coating was prepared on the surface of porous carbon-fiber-reinforced SiCO ceramic composites *via* brushing and sintering method. The gas-penetration resistance of the glass can be enhanced by increasing its viscosity, thus
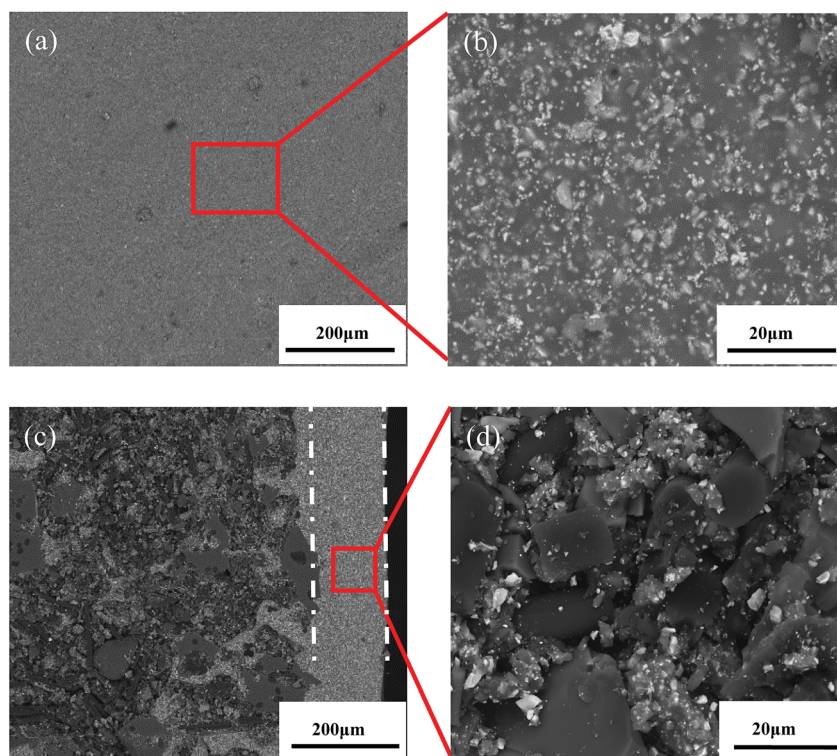

Fig. 2 Surface (a and b) and cross-sectional (c and d) SEM images of the A-TMG coating ((b) and (d) are the partial enlarged detail of the red box in (a) and (c), respectively).
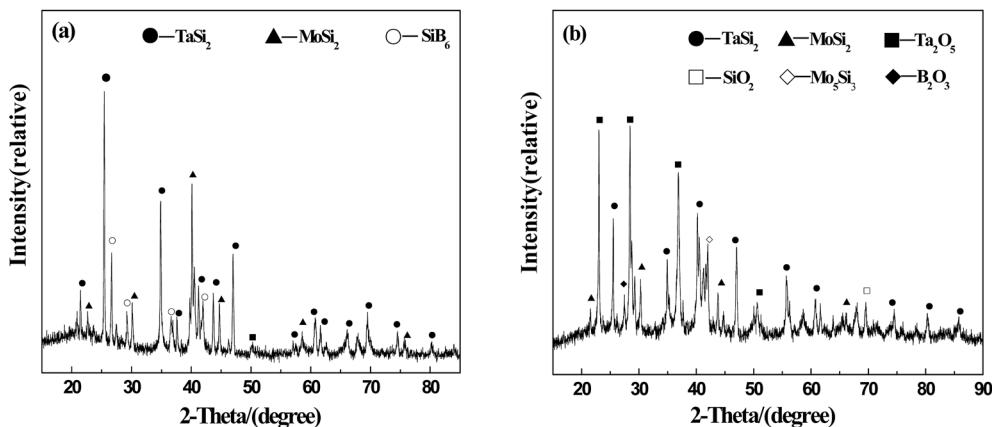
Fig. 3 XRD patterns of the A-TMG coating for inner parts (a) and surface (b).

improving anti-oxidation property of the coating and further protecting the substrate effectively. The microstructure, phase compositions of the coating before and after anti-oxidation test at 1873 K in air were investigated.

2   Experimental

2.1   Materials

Methyltirmethoxysilane (MTMS) and methyldimethoxysilane (DMDES) were purchased from Wuhan Yi Hua Cheng Technology Development Co., Ltd., China. Ethanol (EtOH), nitric acid (HNO_3) and ammonia (NH_4OH) were obtained from Chemical reagent factory of Hunan Normal University. The hard carbon felts were purchased from Hunan Jiuhua Carbon High-Tech Co., Ltd., China, and used as the reinforcement. SiO_2, B_2O_3, Al_2O_3, $TaSi_2$, $MoSi_2$ and SiB_6 powders were all obtained from Sinopharm Chemical Reagent Co., Ltd., China. HNO_3 and NH_4OH were diluted to 0.1 mol l^{-1} and 1 mol l^{-1}, respectively, and other chemical reagents were used as received without purification.

2.2   Preparation of coating

Porous SiCO ceramic composites with a density of 0.55 g cm^{-3} and dimensions of 15 mm × 15 mm × 15 mm were used as the substrates and prepared by precursor impregnation and pyrolysis. The precursor used MTMS and DMDES as monomer, EtOH as solvent, HNO_3 and NH_4OH as catalysts. The prepared composites were hand-polished with 100 grit emery paper before preparing the coatings.

It took three steps to prepare the coating sample. First, preparation of borosilicate glass powder: 80 wt% SiO_2 powder, 15–20 wt% B_2O_3 powder and 0–5 wt% Al_2O_3 powder were ball-milled for 24 h, then placed the mixture in a corundum crucible and heated it in a muffle furnace at 1773 K for 1.5 h. After cooling in the furnace, bulk glass was milled to powders, which were sieved by 300 mesh screen. Second, 40.5 wt% borosilicate glass powder, 50 wt% $TaSi_2$ powder, 7 wt% $MoSi_2$ powder and 2.5 wt% SiB_6 powder (as sintering aids) were dispersed in ethanol and ball-milled for 50 h. Third, the coating slurry was coated on the surface of porous SiCO ceramic

composites by brushing for certain times, then sintered at 1588 K in air for 10 min. The Al_2O_3-containing $TaSi_2$–$MoSi_2$–borosilicate glass (A-TMG) coated porous SiCO ceramic composites were obtained.

2.3   Characterizations

The chemical bonds of the borosilicate glass were determined using a Fourier transform infrared (FTIR) spectrometer (Nicolet Avatar-360). The chemical compositions and elemental distribution of the coated sample were determined using X-ray photoelectron spectroscopy (XPS; ESCA LAB250Xi). Oxidation resistance test was carried out in a KBF 1700 furnace. After the furnace was heated up to 1873 K, the coated sample was placed in it and kept for 20 min. The microstructure and element component of the coating before and after oxidation test were analyzed by a JSM-6460 scanning electron microscopy (SEM) and energy dispersive spectroscopy (EDS). The phase compositions of the coating were determined using X-ray diffraction (XRD; D8 Advance).
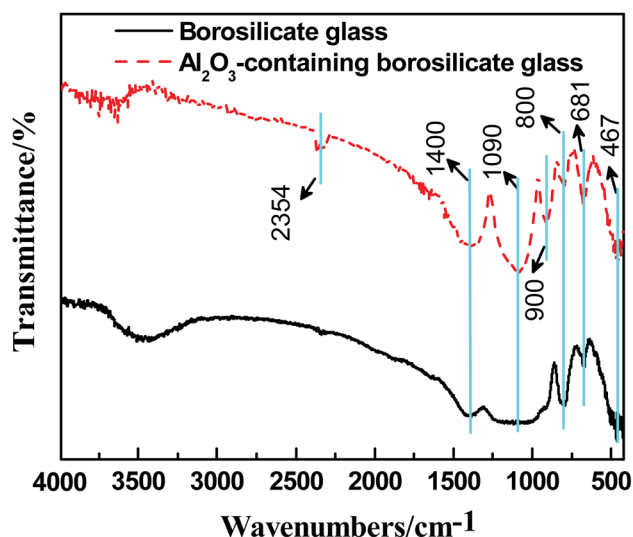

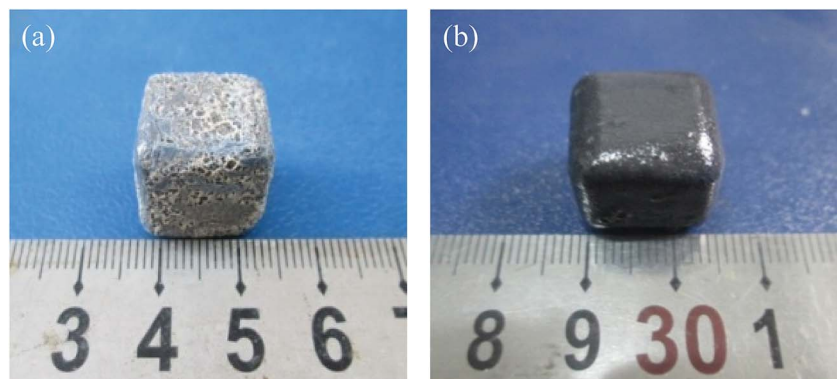**Fig. 4** FTIR spectra of the borosilicate glass with and without Al_2O_3.

Fig. 5 Photographs of the sample coated by TMG (a) and A-TMG (b) after oxidation test.

Table 1 XPS element analysis of the white substances on the TMG coating surface after heated in air at 1873 K for 20 min

Element	Ta4f	Si2p	C1s:C–O	Mo3d	B1s	O1s
Content%	2.45	21.8	21.56	1.51	4.79	47.89

3 Results and discussion

3.1 Microstructure and compositions

The as-prepared coating shows a good macroscopic appearance without deformation and any cracks on the surface (Fig. 1). Compared with the sample coated by $TaSi_2$–$MoSi_2$–borosilicate glass (TMG), the surface of A-TMG coating is more glossy.

To visualize the microstructure of A-TMG coating, the obtained SEM images of the coating surface are shown in Fig. 2a and b. A dense and crack-free surface is observed. Moreover, it can be further seen that the irregular small particles exist as immiscible phases bonded by homogeneous A-TMG phase from the magnification of the coating surface (Fig. 2b). Fig. 2c and d show the cross-sectional SEM images of A-TMG coating, respectively, and the interface between the substrate and the coating is observed therein. The slurry coatings partially infiltrate into the porous structure of the SiCO ceramic composites and are tightly combined with the composites through the continuous glass phase. The coating has a uniform thickness of approximately 180 μm, and no delamination is discovered between the coating and the composites. In the inner coating shown in Fig. 2d, the molten borosilicate glass bonds $TaSi_2$ and $MoSi_2$ particles together while the interior of the coating is not dense.

Phase analysis of A-TMG coating is shown in Fig. 3. Inside the coating, the peaks of $TaSi_2$, $MoSi_2$, and SiB_6 are detected. In addition, the flat peak at around 22° implies that the A-TMG mainly exists in an amorphous form (Fig. 3a).[36] In addition to $TaSi_2$ and $MoSi_2$, Ta_2O_5, Mo_5Si_3, B_2O_3 and SiO_2 are also recognized on as-prepared coating surface, whereas the peak of SiB_6 disappears in the XRD pattern (Fig. 3b). During the fast sintering process in air, $TaSi_2$ and $MoSi_2$ on the surface are partially oxidized to form Ta_2O_5 and Mo_5Si_3. However, the fact that SiB_6 tends to be oxidized above 873 K and is completely oxidized at the sintering temperature is not the only reason for producing B_2O_3 and SiO_2. The fact that the borosilicate glass crystallizes during the cooling process should also be responsible for that.[32,37,39]

Fig. 4 shows the FTIR spectra of the borosilicate glass with and without Al_2O_3. The absorption peak at 467 cm^{-1} is the bending vibration peak of Si–O–Si, and the absorption peak near 800 cm^{-1} is the stretching vibration peak of O–Si–O. The bending vibration peak of Si–O–Si is near 1090 cm^{-1}, which coincides with the anti-symmetric stretching vibration peak of
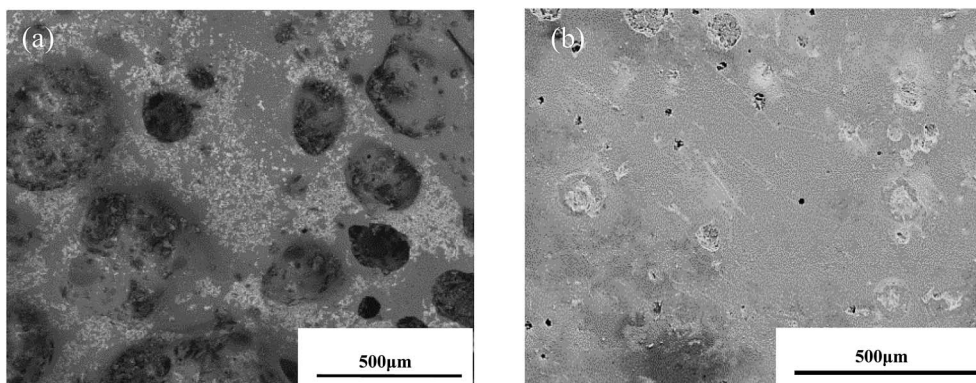

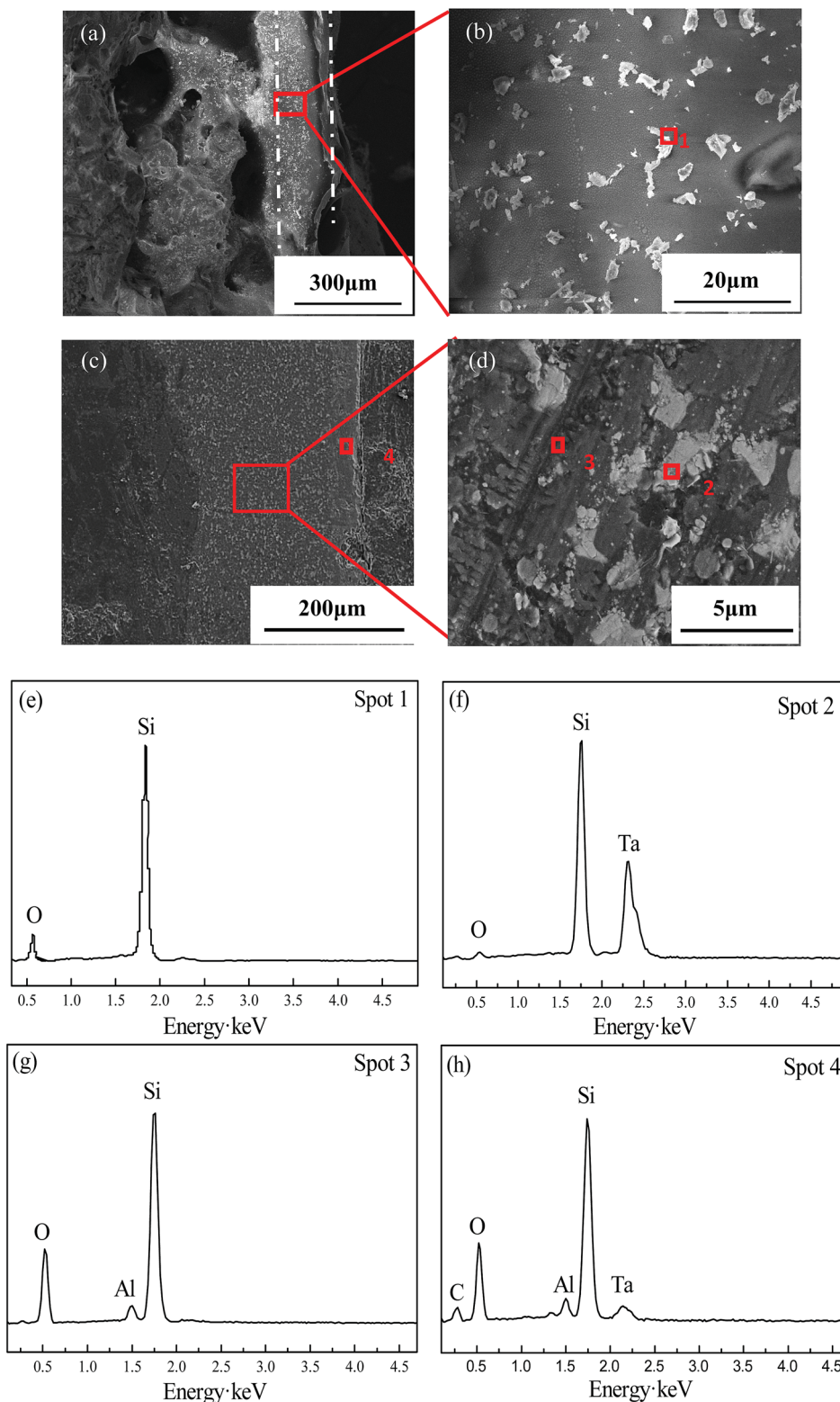**Fig. 6** Surface SEM images of TMG (a) and A-TMG (b) coating after oxidation test.

Fig. 7   Cross-sectional SEM images of TMG (a and b) and A-TMG (c and d) coating after oxidation test and the corresponding EDS analysis (e–h).

$[BO_4]$. In addition, the absorption peaks near 681 cm^{-1} and 1400 cm^{-1} are bending vibration peak and anti-symmetric stretching vibration peak of $[BO_3]$, respectively.[40] From Fig. 4, the peaks at 681 cm^{-1}, 1090 cm^{-1} and 1400 cm^{-1} of the

borosilicate glass with Al_2O_3 are stronger than that without Al_2O_3. Theoretically,[41] when a small amount of Al_2O_3 is added into borosilicate glass, Al^{3+} has priority to capture free oxygen to form $[AlO_4]$, entering the lattice structure of SiO_2 to make the
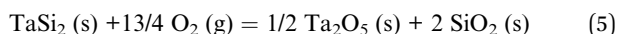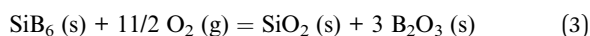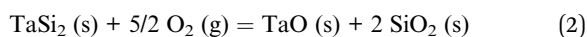
structure more stable. On the other hand, due to the lack of free oxygen, B^{3+} mainly exists in the form of $[BO_3]$ instead of $[BO_4]$. It can be inferred that the introduction of Al_2O_3 makes the borosilicate glass denser and increases the glass viscosity at high temperature.

3.2 Anti-oxidation property

Fig. 5 shows the photographs of the sample after heated in air at 1873 K for 20 min. It can be seen that the TMG coating has poor oxidation resistance at the test temperature. Lots of bulges caused by bubbles burst are overflowed on the coating surface and a large number of white substances are also observed on the coating surface (Fig. 5a). The photograph of the sample coated with A-TMG after oxidation test is presented in Fig. 5b. The sample has a dense and glossy appearance without any cracks. It is believed that the coating can effectively protect porous SiCO composites from oxidation in air at 1873 K after the addition of Al_2O_3.

In our oxidation test, the coating will react with oxygen and the reaction schemes are as follows:[27,35,37]

$$MoSi_2 \text{ (s)} + 7/5 \, O_2 \text{ (g)} = 1/5 \, Mo_5Si_3 \text{ (s)} + 7/5 \, SiO_2 \text{ (s)} \quad (1)$$

$$TaSi_2 \text{ (s)} + 5/2 \, O_2 \text{ (g)} = TaO \text{ (s)} + 2 \, SiO_2 \text{ (s)} \quad (2)$$

$$SiB_6 \text{ (s)} + 11/2 \, O_2 \text{ (g)} = SiO_2 \text{ (s)} + 3 \, B_2O_3 \text{ (s)} \quad (3)$$

$$MoSi_2 \text{ (s)} + 7/2 \, O_2 \text{ (g)} = MoO_3 \text{ (g)} + 2 \, SiO_2 \text{ (s)} \quad (4)$$

$$TaSi_2 \text{ (s)} + 13/4 \, O_2 \text{ (g)} = 1/2 \, Ta_2O_5 \text{ (s)} + 2 \, SiO_2 \text{ (s)} \quad (5)$$

The XPS element analysis of the white substances in Fig. 5a is shown in Table 1. Theoretically, the contents of Ta and Mo before heated in air are 8.02% and 4.96%, respectively. Supposing that all the $TaSi_2$, $MoSi_2$ and SiB_6 are completely oxidized to form solid oxidation products of Ta_2O_5, Mo_5Si_3, SiO_2 and B_2O_3,[42,43] the contents of Ta and Mo should be 5.30% and 3.31%, respectively. However, since the oxidation time is short, there is only a small amount of silicide being oxidized. Thus, the contents of Ta and Mo should be in the range of 5.30–8.02% and 3.31–4.96%, respectively. From Table 1, the contents of both elements are lower than their theoretical minimum while the contents of Si, O and B are relatively high. Therefore, it can be inferred that the main composition of the white substances may be SiO_2–B_2O_3, which is borosilicate glass.[44]

In order to study the microstructure after oxidation test, the surface SEM images of TMG and A-TMG coating after oxidation test are shown in Fig. 6. The TMG coating displays a rough and porous surface with obvious micro defects and holes greater than 200 μm in diameter (Fig. 6a). In contrast, the A-TMG coating surface is smooth with a small number of holes less than 1 μm in diameter (Fig. 6b), indicating that the molten A-TMG coating can fill the microholes and microcracks effectively. Compared with the untested A-TMG coating shown in Fig. 2b, the coating surface becomes denser and more continuous after heated in air at 1873 K, indicating that the formed borosilicate glass heals micro holes by viscous flow.[45]

Fig. 7a shows the cross-sectional SEM images of TMG coating after oxidation test. Along the cross-section, some areas are dense and have a thickness of about 150 μm, but the substrate is badly oxidized and some pores appear. As shown in the magnified SEM images (Fig. 7b), there are a few of white sheet substances within the coating. According to EDS data (Fig. 7e), the white sheet substances are mainly composed of Si and O, indicating the existence of SiO_2.

As is shown in Fig. 7c, the A-TMG coating is still dense, intact and well compacted with the substrates. The coating after oxidation is about 230 μm in thickness and no penetrating holes or visible cracks are observed. A film with a thickness of about 40 μm covers the coating surface, which is in different gray level from the interior of the coating. As far as the interior parts of the coating are concerned, white particles in irregular shapes are surrounded by gray continuous phase (Fig. 7d). The following EDS analysis of the irregular white area (Fig. 7f) indicates that the main elements are Si, Ta and a little O, suggesting that it is a mixture of Ta_2O_5 and non-oxidized $TaSi_2$. The gray continuous phase inside the coating at spot 3 mainly consists of Si, O and Al (Fig. 7g), indicating that it may be molten A-TMG. The reason for the absence of B is that B has a small molecular weight and is difficult to be detected by EDS. The EDS analysis at spot 4 of the surface oxide film (Fig. 7h) shows that the surface comprises Si, Al, Ta and O elements, which suggests that a Ta–Al–Si–O glass layer is generated on the surface of the coating.[27] It can be inferred that the oxide film is mainly composed of SiO_2, Ta_2O_5 and $TaSi_2$. Moreover, the oxidation products cover the coating surface very well and form a dense oxidation layer.

XRD pattern of the A-TMG coating surface after oxidation test is presented in Fig. 8. Besides the $TaSi_2$ phase, Ta_2O_5 diffraction peak with strong intensity can also be detected, which results from the formation of the oxidation product of $TaSi_2$ based on eqn (5). The appearance of crystalline SiO_2 is not only due to oxidation of $TaSi_2$, $MoSi_2$ and SiB_6 at high temperature according to eqn (1)–(5), but also due to crystallization of
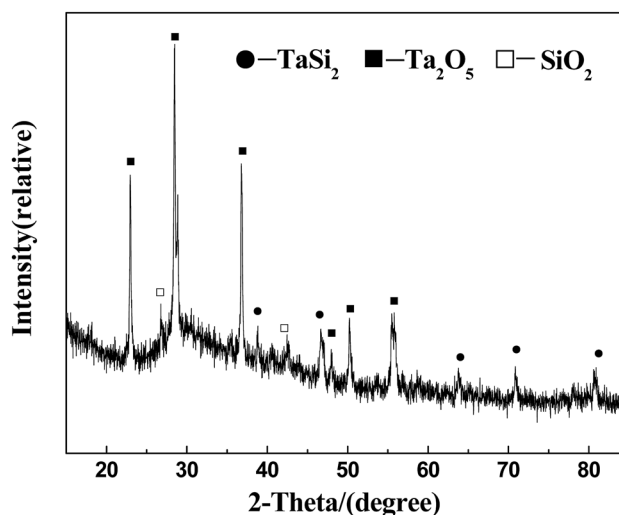

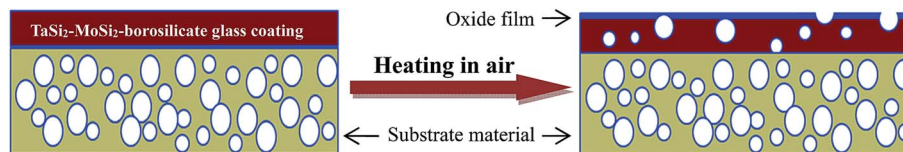Fig. 8 XRD pattern of A-TMG coating surface after oxidation test.

Fig. 9 The failure scheme of TaSi$_2$–MoSi$_2$–borosilicate glass coating under high temperature in air.

some borosilicate glass during subsequent cooling process.[37] Compared to the original XRD pattern of the coating surface (Fig. 3b), the peaks of MoSi$_2$, Mo$_5$Si$_3$ and B$_2$O$_3$ disappear after heated in air at 1873 K for 20 min. The reason for absence of MoSi$_2$ peak is that the amount of MoSi$_2$ is little in the coating slurry so it is completely oxidized at high temperature. Mo$_5$Si$_3$, as the oxidation product of MoSi$_2$, has been further oxidized to generate volatilizable product (MoO$_3$), according to eqn (1) and (4).[27] In addition, the absence of B$_2$O$_3$ and Al$_2$O$_3$ peaks may be due to B$_2$O$_3$ evaporation from original borosilicate glass and the low content of Al$_2$O$_3$.[46]

Fig. 9 shows the failure scheme of the coating at high temperature in air. It is known that the gas inside the porous SiCO ceramic composites tends to expand outside at high temperature. Besides, the complete oxidation of MoSi$_2$ will produce gaseous product, MoO$_3$, which causes pores in the coating. In addition, the coating surface is exposed to air and the oxidation is more serious with an oxide film formed. As we know, the molten borosilicate glass at high temperature has fluidity. Therefore, we believe that the gas penetration resistance of the glass can be enhanced by increasing the glass viscosity through addition of Al$_2$O$_3$. Thus, the silicide in the coating is not easily oxidized and oxidation resistance of the coated sample is improved effectively.

4 Conclusions

A-TMG coating was prepared on the surface of porous carbon fiber reinforced SiCO ceramic composites *via* brushing and sintering. The coated samples show a good macroscopic appearance without deformation and any cracks. From SEM images, the coating with a uniform thickness of approximately 180 μm partially infiltrated into the porous structure of SiCO ceramic composites and bonded the substrate well. After heated in air at 1873 K for 20 min, the A-TMG coating with a film composed of Al$_2$O$_3$, SiO$_2$ and Ta$_2$O$_5$ covering the surface was still dense and intact. The coating was about 230 μm in thickness and no penetrating holes or visible cracks were found. Compared with the TMG coating, the A-TMG coating had a smoother surface after oxidation test, which indicates that oxidation resistance of the coated sample was greatly improved after addition of Al$_2$O$_3$. The reason may be that addition of Al$_2$O$_3$ increased the viscosity of the borosilicate glass at high temperature, and further prevented the substrates from being oxidized by efficiently enhancing the gas penetration resistance of the glass. Thus, the A-TMG coated porous SiCO ceramic composites with excellent anti-oxidation property are potential thermal protection materials for windward surface of hypersonic aircrafts.

Conflicts of interest

There are no conflicts to declare.

Acknowledgements

References

1 D. E. Glass, *AIAA*, 2008-2682.
2 C. L. Yan, R. J. Liu, B. L. Zha and C. R. Zhang, *J. Alloys Compd.*, 2018, **739**, 955.
3 R. T. Voland, L. D. Huebner and C. R. Mcclinton, *Acta Astronaut.*, 2005, **59**, 181.
4 C. L. Yan, R. J. Liu, Y. B. Cao, C. R. Zhang and D. K. Zhang, *Corros. Sci.*, 2014, **86**, 131.
5 E. Lee and K. E. Wurster, *AIAA*, 2017-1146.
6 P. Colombo, *J. Eur. Ceram. Soc.*, 2008, **28**, 1389.
7 H. Tian, Q. S. Ma, Y. Pan and W. D. Liu, *Ceram. Int.*, 2013, **39**, 71.
8 A. H. Tavakoli, M. M. Armentrout, M. Narisawa and S. Sen, *J. Am. Ceram. Soc.*, 2015, **98**, 242.
9 T. Takahashi, H. Munstedt, M. Modesti and P. Colombo, *J. Eur. Ceram. Soc.*, 2001, **21**, 2821.
10 T. H. Xu, Q. S. Ma and Z. H. Chen, *Mater. Lett.*, 2011, **65**, 1538.
11 L. L. Guo, X. Tao, A. R. Guo and J. C. Liu, *Int. Mater. Rev.*, 2016, **30**, 119.
12 L. Bergero, V. M. Sglavo and G. D. Soraru, *J. Am. Ceram. Soc.*, 2005, **88**, 3222.
13 I. Saleh and R. Raj, *J. Power Sources*, 2016, **310**, 18.
14 J. C. Fletcher, A. Pechman and R. M. Beasley, *US Pat.* 3953646, 1976.
15 J. C. Fletcher, A. Pechman and R. M. Beasley, *US Pat.* 3955034, 1976.
16 J. C. Fletcher, H. B. Goldstein and D. B. Leiser, *US Pat.* 4093771, 1978.
17 D. B. Leiser, *Ceram. Eng. Sci. Proc.*, 1981, 809.
18 D. B. Leiser, M. Smith and D. A. Stewart, *Ceram. Eng. Sci. Proc.*, 1983, 551.
19 D. A. Stewart, D. B. Leiser and M. Smith, *Ceram. Eng. Sci. Proc.*, 1983, 533.

20 J. M. Beggs, D. A. Stewart and H. E. Goldstein, *US Pat.* 4381333, 1983.

21 D. B. Leiser, M. Smith and R. A. Churchward, *US Pat.* 5709082, 1992.

22 D. B. Leiser, R. Churchward and V. Katvala, *Ceram. Eng. Sci. Proc.*, 1988, 1125.

23 S. M. Johnson, M. J. Gasch and D. Leiser, AIAA, 2008-2560.

24 D. A. Stewart and D. B. Leiser, *US Pat.* 7314648, 2008.

25 D. A. Stewart, D. B. Leiser, AIAA, 2006-7945.

26 D. B. Leiser, M. T. S. Hsu and T. S. Chen, *US Pat.* 6225248, 2001.

27 G. F. Shao, X. D. Wu, S. Cui, X. D. Shen, Y. C. Lu, Q. H. Zhang and Y. Kong, *J. Alloys Compd.*, 2017, **690**, 63.

28 J. P. Wittenauer, S. D. Reeves, K. W. Benner and R. D. Yasukawa, *US Pat.* 6749942, 2004.

29 D. A. Stewart, D. B. Leiser, R. R. DiFiore and V. W. Katvala, *US Pat.* 7767305B1, 2010.

30 C. H. Wang, R. X. Liu and C. L. Zhou, *J. Adv. Ceram.*, 2014, **354**, 1763.

31 X. Tao, X. J. Xu, L. L. Guo, W. H. Hong, A. R. Guo, F. Hou and J. C. Liu, *Mater. Des.*, 2016, **103**, 144.

32 G. F. Shao, X. D. Wu, S. Cui, X. D. Shen, Y. Kong, Y. C. Lu, C. R. Jiao and J. Jian, *Ceram. Int.*, 2016, **42**, 8140.

33 Q. L. Wen, W. C. Zhou, J. B. Su, Y. C. Qing, F. Luo and D. M. Zhu, *J. Alloys Compd.*, 2016, **666**, 359.

34 J. F. Huang, Y. L. Zhang, K. J. Zhu, L. Y. Cao, C. Y. Li, L. Zhou, H. B. Ouyang, B. Y. Zhang and W. Hao, *J. Alloys Compd.*, 2015, **633**, 317.

35 X. Yong, L. Y. Cao, J. F. Huang, W. H. Kong, J. B. Su, C. Y. Li, H. B. Ouyang, L. Zhou and J. T. Liu, *Surf. Coat. Technol.*, 2017, **311**, 63.

36 X. Tao, X. T. Li, L. L. Guo, X. J. Xu, A. R. Guo, F. Hou and J. C. Liu, *Surf. Coat. Technol.*, 2017, **316**, 122.

37 G. F. Shao, X. D. Wu, Y. Kong, X. D. Shen, S. Cui, X. Guan, C. R. Jiao and J. Jian, *J. Alloys Compd.*, 2016, **663**, 360.

38 L. Wang, Q. G. Fu and F. L. Zhao, *Intermetallics*, 2018, **94**, 106.

39 X. H. Shi, X. R. Zeng, H. J. Li, Q. G. Fu and J. Z. Zou, *Rare Met. Mater. Eng.*, 2011, **40**, 403.

40 Z. X. Chen, J. Quan and Y. M. Zhong, *J. Wuhan Univ. Technol.*, 2009, **31**, 26.

41 X. Q. Liu, H. E. Feng and Y. Fang, *Bull. Chin. Ceram. Soc.*, 2013, **32**, 805.

42 D. S. Hou, K. Z. Li, H. J. Li, Q. G. Fu, Y. L. Zhang and X. T. Li, *Rare Met. Mater. Eng.*, 2009, **38**, 252.

43 J. Matsushita and S. Komarneni, *Mater. Res. Bull.*, 2001, **36**, 1083.

44 G. F. Shao, Y. C. Lu, X. D. Wu, J. Wu, S. Cui, J. Jian and X. D. Shen, *Appl. Surf. Sci.*, 2017, **416**, 805.

45 X. Tao, X. J. Xu, X. Q. Xu, W. H. Hong, A. R. Guo, F. Hou and J. C. Liu, *J. Eur. Ceram. Soc.*, 2017, **37**, 871.

46 J. F. Huang, Y. L. Zhang, K. J. Zhu, C. Y. Li, L. Y. Cao, L. Zhou, H. B. Ouyang, B. Y. Zhang, W. Hao and C. Y. Yao, *Ceram. Int.*, 2015, **41**, 4662.